JBMR Plus, 2024, **8**, ziae106
https://doi.org/10.1093/jbmrpl/ziae106
Advance access publication: August 3, 2024
Research Article

Multi-site phantomless bone mineral density from clinical quantitative computed tomography in males

Zachary A. Haverfield[1,*], Amanda M. Agnew[1], Kathryn Loftis[2], Jun Zhang[3], Lauren E. Hayden[1], Randee L. Hunter[1]

[1]Injury Biomechanics Research Center, The Ohio State University, Columbus, Ohio 43210, United States
[2]United States Army Futures Command DEVCOM Analysis Center, Aberdeen Proving Ground, Maryland, 21005, United States
[3]Medical Physics, The Ohio State University Wexner Medical Center, Columbus, Ohio 43210, United States

*Corresponding author: Zachary A. Haverfield, Injury Biomechanics Research Center, The Ohio State University, 2063 Graves Hall 333 W. 10th Ave., Columbus, Ohio 43210, United States (zachary.haverfield@osumc.edu).

Abstract

Volumetric bone mineral density (vBMD) is commonly assessed using QCT. Although standard vBMD calculation methods require phantom rods that may not be available, internal-reference phantomless (IPL) and direct measurements of Hounsfield units (HU) can be used to calculate vBMD in their absence. Yet, neither approach has been systemically assessed across skeletal sites, and HU need further validation as a vBMD proxy. This study evaluated the accuracy of phantomless methods, including IPL and regression-based phantomless (RPL) calibration using HU to calculate vBMD, compared to phantom-based (PB) methods. vBMD from QCT scans of 100 male post-mortem human subjects (PMHS) was calculated using site-specific PB calibration at multiple skeletal sites throughout the body. A development sample of 50/100 PMHS was used to determine site-specific reference material density for IPL calibration and RPL equations. Reference densities and equations from the development sample were used to calculate IPL and RPL vBMD on the remaining 50/100 PMHS for method validation. PB and IPL/RPL vBMD were not significantly different ($p > .05$). Univariate regressions between PB and IPL/RPL vBMD were universally significant ($p < 0.05$), except for IPL Rad-30 ($p = 0.078$), with a percent difference across all sites of $6.97\% \pm 5.95\%$ and $5.22\% \pm 4.59\%$ between PB and IPL/RPL vBMD, respectively. As vBMD increased, there were weaker relationships and larger differences between PB vBMD and IPL/RPL vBMD. IPL and RPL vBMD had strong relationships with PB vBMD across sites ($R^2 = 97.99$, $R^2 = 99.17\%$, respectively), but larger residual differences were found for IPL vBMD. As the accuracy of IPL/RPL vBMD varied between sites, phantomless methods should be site-specific to provide values more comparable to PB vBMD. Overall, this study suggests that RPL calibration may better represent PB vBMD compared to IPL calibration, increases the utility of opportunistic QCT, and provides insight into bone quality and fracture risk.

Keywords: vBMD, phantomless calibration, QCT, bone quality, internal reference calibration, regression-based calibration

Lay Summary

Quantitative computed tomography (QCT) provides assessments of bone quality using measurements of volumetric bone mineral density (vBMD). Specialized accessories to calculate vBMD (ie, phantom rods) are not always available, so phantomless methods using reference materials within the scan are often utilized. The current study calculated vBMD from 100 males across multiple bones in the body using 2 different methods that do not rely on phantom rods. A development sample of 50 males was used to create internal-reference phantomless (IPL) and regression-based phantomless (RPL) calibration methods, and the remaining 50 were used to validate each method. Both IPL and RPL calibration performed well in comparison to the standard phantom-based approach, but differences in IPL vBMD were larger. These findings indicate that site-specific phantomless methods are trustworthy, but RPL methods may provide better estimates of BMD than IPL methods, especially at denser skeletal sites.

Received: February 16, 2024. **Revised:** July 9, 2024. **Accepted:** August 1, 2024
© The Author(s) 2024. Published by Oxford University Press on behalf of the American Society for Bone and Mineral Research.
This is an Open Access article distributed under the terms of the Creative Commons Attribution Non-Commercial License (https://creativecommons.org/licenses/by-nc/4.0/), which permits non-commercial re-use, distribution, and reproduction in any medium, provided the original work is properly cited.
For commercial re-use, please contact journals.permissions@oup.com

Graphical Abstract

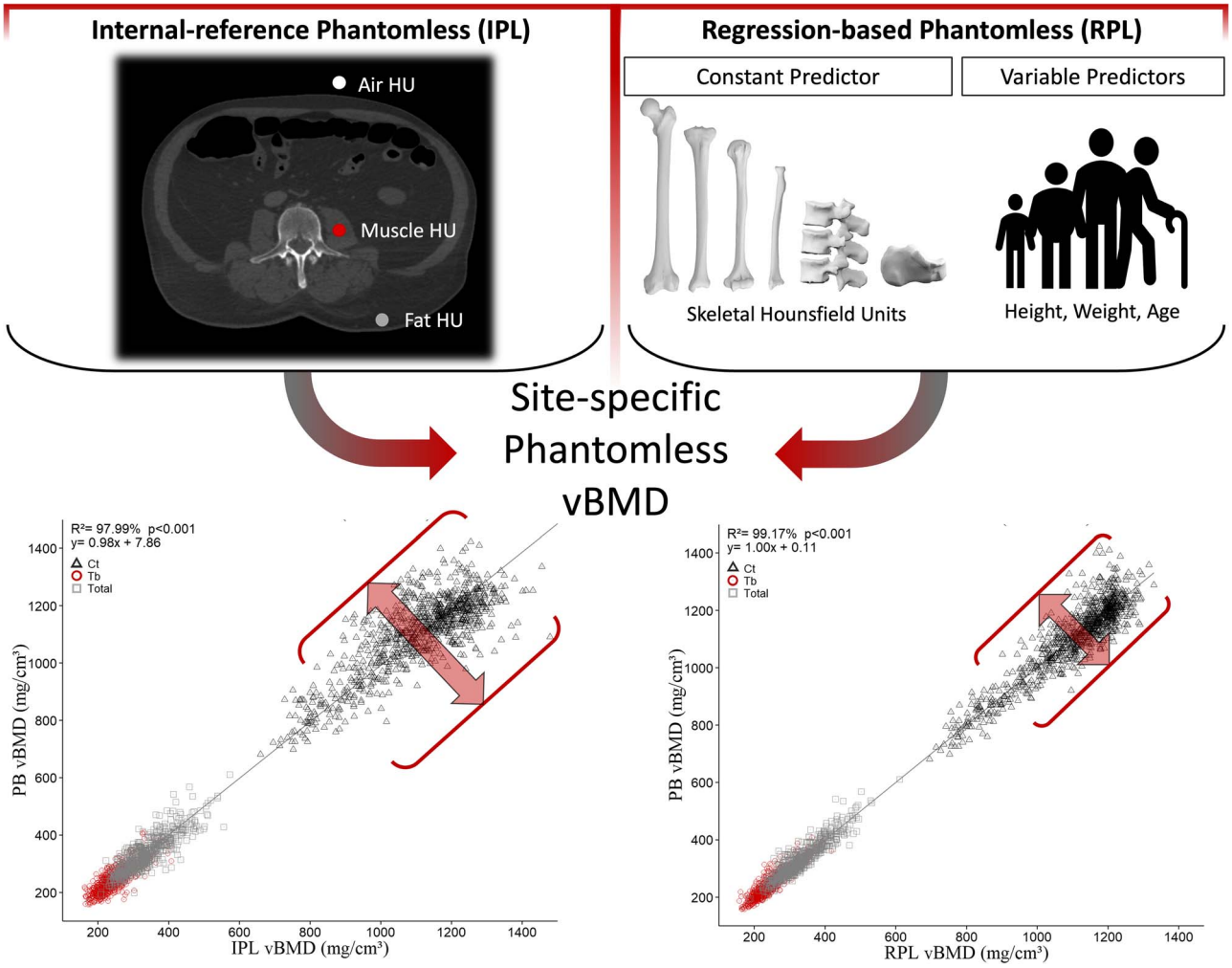

Introduction

Osteoporosis is a global health concern that imparts a heavy societal and economic burden.[1,2] Mortality rates of osteoporotic-related fractures in the pelvis, hip, spine, thorax, and humerus have been reported at 27.3% after 36 mo.[3] Additionally, patients with osteoporotic-related fractures have increased rates of fracture recurrence in the years following their initial injury.[3,4] As these may further increase patient mortality, efforts to standardize alternative methods that identify declining bone quality may drastically reduce the overall impact of osteoporosis[5] and improve the health-related quality of life for patients.

Current clinical assessments of bone quality and fracture risk are primarily conducted using DXA to assess areal bone mineral density (aBMD) at standard locations in the lumbar spine, hip, and distal radius.[6] Despite being the clinical standard, the 2D assessment of aBMD is subject to errors from superimposed hyperdense tissue, which can misrepresent fracture risk.[7-9] Alternatively, QCT can capture volumetric BMD (vBMD)[10,11] and may more accurately represent bone quality than aBMD.[12,13] QCT has been used to identify complex inter- and intra-element variation[12,14-16] and allows for discrimination between cortical and trabecular envelopes.[17] The standard method to calculate vBMD involves the calibration of Hounsfield units (HU) to reference materials of known density, or phantom rods, included in the scan.[18] However, phantom rods are not always available in clinical CT scans, given that the original indication is not often fracture risk assessment. As CT utilization in the medical field increases by almost 8% annually,[19] methods that quantify vBMD without the need for phantom rods may provide additional value to clinical assessments of bone quality.

Methods to calculate vBMD without phantom rods often employ internal-reference phantomless (IPL) calibration utilizing reference values such as air, fat, muscle, and aortic blood. Although these methods can facilitate retrospective analyses of vBMD, they have been explored primarily in the lumbar spine,[20-22] pelvis,[23] and femur.[22,24] Unfortunately, inconsistencies in specific reference materials and their equivalent densities (EqDen) for IPL calibration have been reported across studies.[21,23-25] Regardless of the relationship between HU and material radiodensity within a scan,[26]

using different internal reference materials has been shown to alter the accuracy of IPL compared to phantom-based (PB) vBMD.[27] Furthermore, incorporating reference materials outside of the body (ie, air) with in vivo reference materials (ie, fat, aortic blood, or muscle) has demonstrated less error compared to IPL calibrations that only used in vivo reference materials.[24,27,28] However, this has only been explored within the lumbar spine[27] and does not account for the influence of differential relative X-ray attenuation[29,30] or significant differences in EqDen values throughout the body.[31] As these influences may introduce error in phantomless calibration curves to quantify vBMD and resulting assumptions of fracture risk, additional research is required to determine the accuracy of IPL HU calibration across skeletal sites.

In contrast to IPL methods, opportunistic CT[32] is another retrospective phantomless (PL) methodology that utilizes skeletal HU values as a metric of bone quality.[33] Previous research has investigated the use of skeletal HU as a proxy for DXA-derived BMD.[33-35] However, BMD measured between DXA and QCT may not be comparable[12,36] and may not be appropriate for the development of PL methods. In addition, HU measured from QCT are subject to the influence of CT acquisition parameters such as kVp,[37] different scanner manufacturers,[38] and relative tissue thickness[39] that varies throughout the body. Although prior research has used HU (eg, air, bone, muscle, fat, blood) in a multiple regression technique to calculate vBMD,[20,40] further research is needed to explore the appropriateness of using primarily skeletal HU as a proxy measure of QCT vBMD across multiple skeletal sites and tissue types.

Quantitative assessments of vBMD using QCT demonstrate promising practical and clinical utility that may improve the accuracy and sensitivity of identifying populations at risk of fracture. However, vBMD varies throughout the body and by tissue type (ie, trabecular and cortical bone),[12] suggesting these methods likely require site-specific approaches.[41] Historically, PL methods used to calculate vBMD have primarily been limited to the lumbar spine, pelvis, and femur, and using HU as a direct measure of BMD has also not been explored within the context of QCT across the skeleton. Therefore, the purpose of this study was to evaluate the accuracy of PL vBMD calculation methods, including site-specific IPL and *regression-based phantomless* (RPL) calibration methods, against PB methods at varying skeletal sites and tissue types.

Materials and methods

Sample and data collection

One-hundred male post-mortem human subjects (PMHS) ranging in age from 24 to 102 yr and without skeletal pathology were utilized for this study (Table 1). The sample was randomly divided into a method *development* ($n = 50$) and method *validation* ($n = 50$) sample while maintaining similar age distributions (2 sample *t*-test, $p > .05$). Whole body QCT scans of each PMHS were conducted shortly after death on either a 384-slice Siemens Somatom Force with a spatial resolution of 0.24 mm or a 128-slice Siemens Somatom Definition Edge with a spatial resolution of 0.3 mm (CV:1.92%, LSC: 5.32%). Acquisition parameters of 120 kVp (tin filter) and a 250-reference mA were used with an abdomen protocol and a collection diameter of 500 mm onto a 512 × 512 matrix. Each scan included INTable phantom rods of known densities (0–150 mg/cm^3) that were used to generate site-specific HU to vBMD calibration curves.

Volumes of interest (VOIs) were obtained using blunt segmentation in OsiriX MD imaging software (v.12.0.02) from multiple skeletal locations throughout the body, including the left humerus, radius, femoral neck, midshaft femur, tibia, and calcaneus, as well as the second to fourth lumbar vertebrae (Figure 1). Each VOI included 5 axial slices (0.6 mm slice thickness for an in-plane volume of 3 mm of bone) except for those obtained from the femoral neck, which was segmented into 3 coronal slices (1.3 mm slice thickness for an in-plane volume of 3.9 mm of bone) for accurate visualization of the anatomy. Multiple sites along the diaphysis of the radius and tibia were analyzed to account for varying skeletal composition and soft tissue thickness (Figure 1). Consistent HU thresholds were applied to each VOI to analyze only bone voxels for separate measures of trabecular (Tb) (150–660 HU), cortical (Ct) (661–3000 HU), and total vBMD (150–3000 HU) (Table 2).[30,42,43]

To determine the necessity of site-specific PB calibration when calculating vBMD, an initial investigation was performed on $n = 50$ PMHS, which were randomly selected from the whole sample. Two approaches were used: (1) site-specific PB calibration and (2) general PB calibration where HU from the phantom rods were obtained from the location of the L3 VOI and used to calculate vBMD for a subset of VOIs (Hum-50, Rad-50, L2 and L4, all Fem-N VOIs, and Tib-50). These sites were selected to include extremities that may represent regions of differential X-ray attenuation (Hum, Rad, and Tib-50) as well as VOIs where skeletal HU was obtained from the coronal plane (Fem-N). It was hypothesized that differences between vBMD calculated from site-specific phantom calibration curves (SS-Cal) and general phantom calibration curves (Gen-Cal) would be larger the farther the anatomical VOI was from the location of L3. Paired *t*-tests were used to assess differences in mean vBMD between SS-Cal and Gen-Cal methods and demonstrated significant differences at sites farther away from the location of L3 ($p < 0.05$) (Table SS1). As expected, VOIs in the same region as L3 used for the Gen-Cal (Rad, L2, L4) yielded similar vBMD ($p > 0.39$). This exploration suggested that X-ray attenuation from the individual differentially affected vBMD calculations supporting the necessity of site-specific calibration curves to reduce error in vBMD calculations. Therefore, PB vBMD from the *whole sample* for this study utilized site-specific calibration curves to calculate vBMD at each VOI. Additionally, the concept of site-specificity was applied for both PL vBMD calibration methods tested here.

PL calibration and statistical analyses

Calculations of site-specific vBMD were conducted using a custom MATLAB (MathWorks v.9.11.0) code. All statistical analyses were performed in MiniTab statistical software (v.21.3.1) with an a priori alpha level of $p < 0.05$. Prior to analyses, phantom rod HU values, when scanned independently, were compared to assess any baseline differences between the two scanners used in this study. Two sample *t*-tests between each phantom rod demonstrated that the Somatom Force scanner had significantly higher HU values than the Somatom Definition Edge ($p < 0.001$). As a result, scanner type was accounted for in all analyses.

The *IPL calibration* method was performed on the development sample. Reference HU values from air, fat, and muscle were obtained from regions surrounding each skeletal site using typical HU thresholds for fat (−190 to −30 HU) and muscle (−29 to 149 HU).[30,44] Generating a PL calibration

Table 1. Sample demographics and CT scanner frequency.

Variable	Whole sample Mean ± SD $n = 100$	Development sample Mean ± SD $n = 50$	Validation sample Mean ± SD $n = 50$
Age (yr)	62.57 ± 13.04	62.12 ± 12.92	63.02 ± 13.27
Height (cm)	176.60 ± 6.75	175.48 ± 6.93	177.72 ± 6.44
Weight (kg)	74.04 ± 10.64	73.95 ± 10.19	74.13 ± 11.18
Somatom Force (n)	76	40	36
Somatom Definition Edge (n)	24	10	14

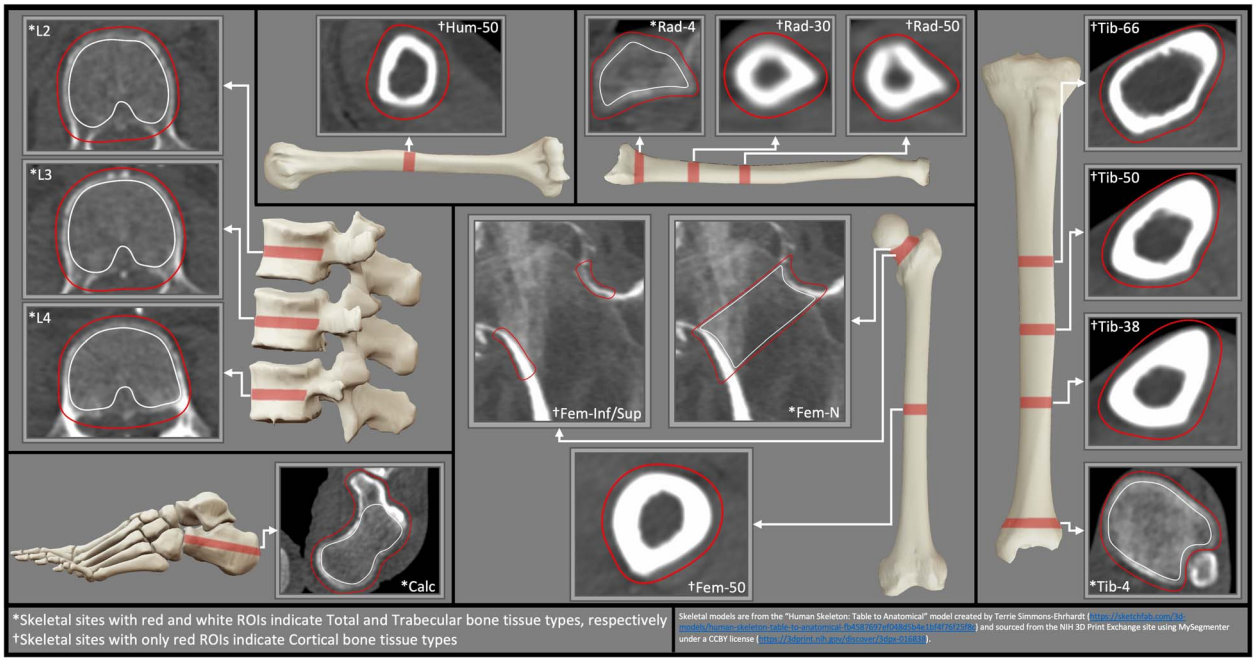

Figure 1. Locations of skeletal VOI collection and exemplar cross-sections of ROIs from each skeletal site of interest.

Table 2. Skeletal volumes of interest and tissue types.

Skeletal element	Site(s)[a]	Abbreviation(s)	Skeletal tissue type(s)
Humerus	50%	Hum-50	Ct
Radius	4%	Rad-4	Tb, Total
Radius	30%, 50%	Rad-30, Rad-50	Ct
2nd-4th Lumbar Spine	Mid	L2, L3, L4	Tb, Total
Femoral Neck	Mid	Fem-N	Tb, Total, Ct (Inf, Sup)
Femur	50%	Fem-50	Ct
Tibia	4%	Tib-4	Tb, Total
Tibia	38%, 50%, 66%	Tib-38, Tib-50, Tib-66	Ct
Calcaneus	Mid	Calc	Tb, Total

[a]Sites obtained within the axial plane are defined as either a percentage of total length relative to the distal end or from the axial midpoint (mid) (50%) of the skeletal element. The femoral neck site was defined at the coronal midpoint (mid) (50%) of the skeletal element. Abbreviations: Ct, cortical bone; Tb, trabecular bone; Inf, inferior cortex; Sup, superior cortex.

curve from these internal references requires known EqDen of each respective reference medium. As there are no consistently reported ground-truth densities of air, fat, or muscle, HU from respective reference VOIs of the method development sample at each skeletal site were converted to an equivalent vBMD using PB calibration curves. The site-specific equivalent density (EqDen) of air, fat, and muscle was averaged across the development sample of 50 PMHS specific to each scanner (Table 3). Using an approach similar to PB calibration, the HU values of air, fat, and muscle were plotted against their calculated EqDen to create a PL calibration equation for each PMHS at every skeletal site (Figure 2). The resulting regression equations were used to calculate vBMD from the mean HU of each skeletal VOI in the validation sample.

RPL calibration method was performed on the development sample and used a backwards-elimination stepwise multiple regression approach. In each regression, site-specific HU was included with additional variables of PMHS weight (kg), height (cm), and age (yr), which were used to refine the model at each iteration. To account for variability in the quality of the CT X-ray tube, scanner type (Somatom Force or Definition Edge) was included as a categorical variable. At each step, the

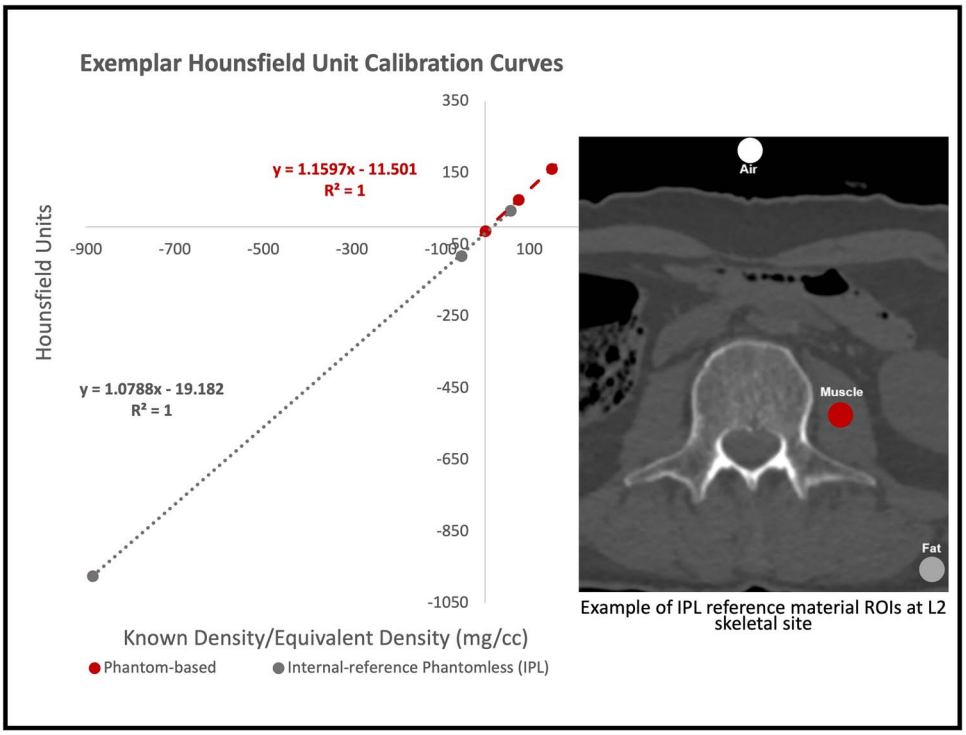

Figure 2. Exemplar phantom-based (PB) and internal-reference phantomless (IPL) HU calibration curves from L2 VOI.

non-significant variable ($p>0.05$) with the least contribution to the model was removed. This process was repeated until all non-significant variables were either removed or if skeletal HU and scanner type were the only predictors remaining. HU data for site-specific regressions are independent of HU from other skeletal sites. The resulting RPL regression equations from the development sample were used to calculate vBMD in the validation sample to evaluate the accuracy of this method across multiple skeletal sites and tissue types.

Kruskal–Wallis (KW) tests evaluated differences in EqDen values of air, fat, and muscle between scanners in the development sample to isolate their potential influences on calculations of IPL vBMD. To assess the ability of IPL and RPL methods to predict PB vBMD at each skeletal site (with respect to tissue type), univariate regressions were used to compare PL and PB vBMD in the validation sample. Additionally, paired *t*-tests were used to assess differences in mean vBMD values between PL and PB. To evaluate the accuracy of these methods across the HU scale (low to high HU), IPL and RPL methods were compared to PB vBMD at all sites using univariate regressions. To assess differences between the spread of IPL and RPL vBMD, method-specific residuals were evaluated using Bonett tests of two variances.

Results

Development vs validation sub-samples

All skeletal HU data were normally distributed (Kolmogorov–Smirnov, $p>0.05$). No significant differences were observed for PB vBMD at any site between the development and validation samples (two sample *t*-test, $p>0.05$).

IPL calibration

Site- and scanner-specific EqDen values from the method development sample (Table 3) were used for IPL vBMD calculations of the method validation sample. When assessing EqDen values of air, fat, and muscle between the two scanners, significant differences were observed across all reference materials ($p<0.05$) but not across all skeletal sites. As a result, site- and scanner-specific EqDens were used for all reference materials in the IPL calibration curve.

Using site- and scanner-specific EqDen values, IPL vBMD was calculated for each skeletal VOI in the validation sample and compared to PB vBMD. No significant differences were observed between IPL and PB vBMD at any skeletal site (paired *t*-test, $p>0.05$) (Table 4) (Figure SS1). Similarly, IPL vBMD significantly predicted PB vBMD at all sites (linear regression, $p<0.05$), except for Rad-30 ($p=0.078$), with the strongest and weakest relationships observed at the Calc Total ($R^2=67.90\%$) and Tib-38 ($R^2=8.59\%$) sites, respectively (Table 4) (Figure SS1). Overall, IPL vBMD had an average percent difference of $6.97\pm5.95\%$ and an absolute magnitude difference of 38.84 ± 43.96 (mg/cm^3) from PB vBMD.

RPL calibration

RPL phantomless regressions generated for each skeletal site by tissue type in the development sample are reported in Table 5. All final RPL regression models significantly predicted PB vBMD ($p<0.05$). For some sites in the extremities (ie, tibia and calcaneus), following the process of backwards-elimination, final regression equations included only HU and scanner type to predict PB vBMD. In contrast, sites closer to the trunk of the body incorporated HU, weight, height (except for Hum-50), and scanner type as significant predictors in the model. None of the final regression equations included age as a significant predictor in the model. Generally, higher R^2 values were observed in models specific to Tb and Total compared to Ct bone tissue-types. Overall, the development of RPL calibration equations revealed the strongest prediction of PB vBMD in the Fem-N Tb site ($R^2_{Adj}=85.12\%$), while the

Table 3. Site and scanner-specific equivalent densities of air, fat, and muscle VOIs (development sample).

Skeletal sites[a]	Air EqDen (mg/cm^3)			Fat EqDen (mg/cm^3)			Muscle EqDen (mg/cm^3)		
	Force Mean ± SD	Edge Mean ± SD	KW test *p*-value	Force Mean ± SD	Edge Mean ± SD	KW test *p*-value	Force Mean ± SD	Edge Mean ± SD	KW test *p*-value
Hum-50	−879.74 ± 59.83	−964.02 ± 82.93	**0.004**	−63.32 ± 19.93	−62.57 ± 14.41	0.594	68.36 ± 19.10	73.13 ± 22.90	0.224
Rad-50	−878.65 ± 49.64	−941.67 ± 97.94	0.085	−57.41 ± 16.88	−55.37 ± 20.90	0.827	56.94 ± 15.25	58.01 ± 25.49	0.680
Rad-30	−874.39 ± 66.32	−951.34 ± 72.27	**0.004**	−54.28 ± 18.11	−52.86 ± 18.69	0.513	62.94 ± 19.31	60.34 ± 24.98	0.846
Rad-4	−865.94 ± 55.59	−950.62 ± 86.39	**<0.001**	−57.55 ± 15.36	−45.52 ± 11.94	**0.008**	57.72 ± 23.46	61.94 ± 19.15	0.332
L2	−864.51 ± 58.01	−968.44 ± 59.76	**<0.001**	−56.54 ± 16.04	−41.29 ± 6.80	**0.002**	54.69 ± 17.13	66.40 ± 19.13	**0.042**
L3	−868.08 ± 73.63	−976.26 ± 9.92	**<0.001**	−56.93 ± 18.90	−45.47 ± 14.30	**0.037**	57.89 ± 16.60	65.40 ± 20.35	0.109
L4	−861.27 ± 61.55	−930.17 ± 106.91	**0.035**	−57.07 ± 16.88	−47.78 ± 13.66	0.069	57.92 ± 15.14	59.32 ± 19.91	0.174
Fem-N	−892.27 ± 47.94	−946.02 ± 77.25	0.055	−61.85 ± 14.95	−44.06 ± 17.60	**0.003**	52.33 ± 19.25	63.92 ± 18.60	**0.029**
Fem-50	−835.10 ± 59.19	−923.84 ± 66.42	**0.001**	−54.08 ± 18.00	−49.47 ± 19.56	0.370	67.15 ± 21.64	65.07 ± 21.82	0.771
Tib-66	−805.70 ± 42.91	−882.22 ± 66.12	**<0.001**	−51.62 ± 17.26	−54.47 ± 21.09	0.961	51.58 ± 19.84	48.58 ± 12.39	0.903
Tib-50	−801.07 ± 27.75	−867.16 ± 60.78	**<0.001**	−51.62 ± 18.45	−53.52 ± 16.78	0.942	49.45 ± 20.37	53.07 ± 10.68	0.190
Tib-38	−788.52 ± 44.48	−869.83 ± 59.24	**<0.001**	−47.03 ± 21.66	−50.64 ± 19.27	0.554	50.47 ± 15.98	50.24 ± 16.62	0.884
Tib-4	−787.44 ± 44.73	−876.79 ± 62.60	**<0.001**	−47.46 ± 14.55	−44.65 ± 13.06	0.383	45.70 ± 18.32	41.52 ± 11.05	0.467
Calc	−812.85 ± 44.50	−896.69 ± 127.24	**0.010**	−44.28 ± 18.70	−44.00 ± 15.38	0.923	55.28 ± 23.85	59.97 ± 13.84	0.528

Abbreviations: EqDen, equivalent densities; KW, Kruskal–Wallis; VOI, volumes of interest. [a]Skeletal sites that have multiple tissue types utilize the same EqDen values (eg, L2 Tb and L2 Total use EqDen values from L2). **Bold** = Statistical significance p<0.05.

weakest prediction was observed at Tib-50 (R^2_{Adj} = 26.00%) (Table 5). Supplemental RPL regressions were conducted and included only skeletal HU and scanner type (Table SS2). These analyses demonstrate similar but slightly weaker relationships than the regressions in Table 5 and represent the isolated relationship between HU and vBMD for sites (Table 5).

The RPL regression equations established from the development sample were used to calculate RPL vBMD for each VOI and tissue type in the validation sample (n = 50). When comparing RPL and PB vBMD, no significant differences were observed between the two methods (p>0.05). RPL vBMD had an average percent and an absolute magnitude difference of 5.22 ± 4.59% and 27.67 ± 30.46 (mg/cm^3), respectively. All relationships between RPL vBMD and PB vBMD were statistically significant (linear regression, p<0.05). The strongest relationship between RPL and PB methods was observed in Fem-N Total vBMD (R^2 = 81.47%), while the weakest was Tib-38 (R^2 = 12.14%) (Figure SS2). Similar to the development sample, higher R^2 values were generally observed for Tb and Total bone compared to Ct bone (Table 6).

PL vs PB method comparisons

Within the validation sample, site-specific vBMD of all VOIs from both IPL and RPL methods were compared to PB vBMD to discern overall differences between each PL method across all skeletal tissue types. Both IPL and RPL vBMD demonstrated a strong significant relationship with PB vBMD (R^2 = 97.99%, p<0.001 and R^2 = 99.17%, p<0.001, respectively) (Figure 3). Bonnet tests demonstrated significantly different variances of residuals in the IPL and the RPL vBMD (p<0.001) with the distribution of these residuals being greater in the IPL method. Bland Altman plots demonstrated that 7.00% and 6.17% of the PL and PB comparisons were beyond the levels of agreement for IPL and RPL vBMD, respectively (Figure 4). The distribution of residual differences increased with increasing densities of vBMD (ie, cortical bone) and demonstrated no consistent over/under prediction of PB vBMD (Figure 4).

Discussion

To evaluate the universal applicability of PL methods, this study utilized multiple skeletal sites and methodologies (IPL and RPL) for calculating vBMD. Site-specific IPL vBMD calibration within this study included both air and in vivo reference materials (ie, fat and muscle) to minimize potential differential influences across the body. Similarly, site-specific RPL vBMD calibration was also conducted to improve the application of this method across the body and between individuals by utilizing subject-specific factors that may account for differential X-ray attenuation. As previous methods of PL vBMD calibration have not explored these approaches across multiple skeletal sites and tissue types, this study offers a unique perspective for more standardized and applicable PL assessments of vBMD.

Results from this study demonstrated that both IPL and RPL vBMD calibration produced measurements of trabecular, total, and cortical vBMD that were strongly related to PB vBMD. Previous research using IPL calibration techniques found strong relationships between PB and IPL vBMD in the lumbar spine,[20-22] pelvis,[23] and the femur[22,24] but did not investigate RPL methods on the same samples for direct comparison of the performance of PL methods. In this study,

Table 4. Internal-reference phantomless assessment (validation sample).

Skeletal sites	Paired *t*-test				Univariate regression	
	PB vBMD (mg/cm^3) Mean ± SD	IPL vBMD (mg/cm^3) Mean ± SD	Percent difference (%)	*p*-value	R^2 (%)	*p*-value
Hum-50	1142.52 ± 89.82	1130.64 ± 86.35	6.01 ± 4.67	0.340	26.05	**<0.001**
Rad-50	1112.09 ± 87.43	1128.12 ± 99.85	7.76 ± 6.33	0.315	8.63	**0.038**
Rad-30	1105.06 ± 63.93	1106.00 ± 88.80	6.37 ± 5.79	0.945	6.31	0.078
Rad-4 Tb	240.98 ± 37.68	237.72 ± 41.59	8.05 ± 7.52	0.397	59.89	**<0.001**
Rad-4 Total	305.04 ± 38.32	301.53 ± 45.41	7.34 ± 7.14	0.438	52.54	**<0.001**
L2 Tb	220.91 ± 34.59	220.09 ± 35.57	9.07 ± 6.99	0.820	54.33	**<0.001**
L2 Total	296.36 ± 38.33	294.15 ± 42.88	7.96 ± 6.15	0.614	51.38	**<0.001**
L3 Tb	221.47 ± 30.13	226.11 ± 26.55	8.77 ± 6.30	0.097	48.00	**<0.001**
L3 Total	303.27 ± 35.60	308.37 ± 36.82	7.66 ± 5.23	0.473	48.22	**<0.001**
L4 Tb	233.43 ± 30.80	234.53 ± 27.53	9.60 ± 7.52	0.585	24.58	**<0.001**
L4 Total	320.29 ± 36.33	322.50 ± 37.29	8.49 ± 7.37	0.879	24.21	**<0.001**
Fem-N Tb	295.09 ± 45.60	292.54 ± 43.44	8.33 ± 6.43	0.581	54.13	**<0.001**
Fem-N Total	421.67 ± 61.89	418.18 ± 65.22	7.22 ± 6.22	0.553	62.46	**<0.001**
Fem-N Sup	853.45 ± 83.53	844.47 ± 81.01	6.53 ± 5.72	0.401	34.19	**<0.001**
Fem-N Inf	1011.87 ± 85.29	1002.28 ± 102.26	6.42 ± 5.64	0.456	30.12	**<0.001**
Fem-50	1197.74 ± 67.74	1211.68 ± 71.99	4.83 ± 4.20	0.204	16.13	**0.004**
Tib-66	1154.28 ± 69.12	1162.26 ± 77.50	4.84 ± 4.04	0.453	23.87	**<0.001**
Tib-50	1195.23 ± 60.83	1207.33 ± 85.10	5.15 ± 3.76	0.268	24.23	**<0.001**
Tib-38	1215.48 ± 61.11	1201.35 ± 80.30	5.17 ± 4.61	0.248	8.59	**0.039**
Tib-4 Tb	247.43 ± 35.88	247.71 ± 35.72	6.33 ± 5.02	0.927	66.39	**<0.001**
Tib-4 Total	294.33 ± 39.72	294.46 ± 40.01	5.85 ± 4.86	0.970	67.39	**<0.001**
Calc Tb	226.78 ± 30.61	227.76 ± 35.36	6.96 ± 5.69	0.738	66.36	**<0.001**
Calc Total	367.75 ± 43.21	369.43 ± 48.16	5.51 ± 4.75	0.669	67.90	**<0.001**

Abbreviations: PB, phantom-based; IPL, internal-reference phantomless; vBMD, volumetric bone mineral density. **Bold** = Statistical significance $p<0.05$.

Table 5. Regression-based phantomless regression results (development sample).

Skeletal VOIs	Equation coefficients					R^2_{Adj} (%)	*p*-value
	Constant	Hounsfield units	Weight	Height	Scanner[a]		
Hum-50	77.50	0.79	2.77		−89.75	55.50	**<0.001**
Rad-50	514.25	0.84	2.44	−2.72	−104.17	56.20	**<0.001**
Rad-30	507.45	0.80	2.86	−2.69	−79.24	66.42	**<0.001**
Rad-4 Tb	123.20	0.97	1.14	−0.95	−31.67	70.70	**<0.001**
Rad-4 Total	161.75	0.96	1.25	−1.16	−38.58	72.53	**<0.001**
L2 Tb	149.46	0.84	1.09	−0.94	−29.58	74.88	**<0.001**
L2 Total	124.02	0.97	1.36	−1.03	−38.18	82.44	**<0.001**
L3 Tb	157.58	0.84	1.20	−1.03	−31.20	75.62	**<0.001**
L3 Total	135.04	0.99	1.52	−1.20	−38.68	80.11	**<0.001**
L4 Tb	156.25	0.87	1.22	−1.08	−27.04	69.17	**<0.001**
L4 Total	161.74	0.94	1.51	−1.28	−36.01	74.07	**<0.001**
Fem-N Tb	185.02	0.89	1.27	−1.23	−33.22	85.12	**<0.001**
Fem-N Total	231.62	0.90	1.59	−1.58	−38.35	80.40	**<0.001**
Fem-N Sup	582.94	0.73	2.78	−3.04	−61.64	66.98	**<0.001**
Fem-N Inf	584.41	0.79	2.94	−3.16	−73.00	58.75	**<0.001**
Fem-50	747.37	0.60	3.65	−3.14	−72.94	37.06	**<0.001**
Tib-66	791.51	0.53	1.56	−2.34	−65.12	38.28	**<0.001**
Tib-50	568.90	0.54			−56.17	26.00	**<0.001**
Tib-38	666.93	0.42			−65.16	36.57	**<0.001**
Tib-4 Tb	67.80	0.72			−22.47	72.08	**<0.001**
Tib-4 Total	66.45	0.76			−27.32	74.17	**<0.001**
Calc Tb	67.48	0.74			−23.62	63.83	**<0.001**
Calc Total	54.87	0.87			−41.75	70.28	**<0.001**

Abbreviations: PB, phantom-based; RPL, regression-based phantomless; vBMD, volumetric bone mineral density; VOI, volumes of interest. **Bold** = Statistical significance $p<0.05$ [a]Scanner coefficients were calculated for the Somatom force when the definition edge was held at zero.

the strength of the relationship between IPL/RPL vBMD and PB vBMD varied between skeletal sites. For instance, skeletal VOIs from the humerus and distal radius demonstrated smaller absolute differences to PB vBMD when using IPL calibration, while all other skeletal VOIs showed smaller differences when using RPL calibration. These findings are congruent with previous results from Bartenschlager and colleagues[40] who reported smaller differences between PB and PL vBMD in the lumbar spine when using a multiple regression approach (RPL) compared to using EqDen of reference materials (IPL). Although results from the current study demonstrated strong linear relationships between PB and IPL vBMD in the lumbar spine, works from Weaver et al. and Prado et al. found stronger relationships at this anatomical site

Table 6. Regression-based phantomless assessment (validation sample).

Skeletal sites	Paired *t*-test				Univariate regression	
	PB vBMD (mg/cm^3) Mean ± SD	RPL vBMD (mg/cm^3) Mean ± SD	Percent difference (%)	*p*-value	R^2 (%)	*p*-value
Hum-50	1142.52 ± 89.82	1141.83 ± 62.10	4.50 ± 4.20	0.947	35.20	**<0.001**
Rad-50	1112.09 ± 87.43	1110.07 ± 62.57	4.14 ± 3.55	0.829	43.73	**<0.001**
Rad-30	1105.06 ± 63.93	1101.87 ± 55.18	3.64 ± 2.74	0.664	40.06	**<0.001**
Rad-4 Tb	240.98 ± 37.68	241.81 ± 40.55	6.76 ± 5.75	0.808	66.07	**<0.001**
Rad-4 Total	305.04 ± 38.32	306.42 ± 41.24	6.06 ± 5.24	0.710	61.84	**<0.001**
L2 Tb	220.91 ± 34.59	219.97 ± 32.70	6.82 ± 5.64	0.739	68.33	**<0.001**
L2 Total	296.36 ± 38.33	296.24 ± 40.81	5.83 ± 5.10	0.971	66.99	**<0.001**
L3 Tb	221.47 ± 30.13	223.55 ± 26.85	6.87 ± 5.80	0.464	57.80	**<0.001**
L3 Total	303.27 ± 35.60	305.81 ± 40.72	5.83 ± 4.73	0.436	68.69	**<0.001**
L4 Tb	233.43 ± 30.80	233.35 ± 24.18	6.97 ± 5.51	0.978	48.91	**<0.001**
L4 Total	320.29 ± 36.33	321.07 ± 33.74	5.98 ± 4.38	0.826	55.42	**<0.001**
Fem-N Tb	295.09 ± 45.60	292.84 ± 37.99	6.07 ± 4.65	0.494	74.52	**<0.001**
Fem-N Total	421.67 ± 61.89	417.83 ± 60.44	5.11 ± 3.85	0.321	81.47	**<0.001**
Fem-N Sup	853.45 ± 83.53	843.63 ± 70.28	4.26 ± 3.18	0.134	70.28	**<0.001**
Fem-N Inf	1011.87 ± 85.29	1004.03 ± 70.74	4.09 ± 3.03	0.303	61.23	**<0.001**
Fem-50	1197.74 ± 67.74	1207.65 ± 51.87	4.00 ± 3.25	0.257	25.34	**<0.001**
Tib-66	1154.28 ± 69.12	1145.76 ± 43.84	4.12 ± 3.69	0.377	12.38	**0.012**
Tib-50	1195.23 ± 60.83	1202.35 ± 36.26	3.30 ± 2.73	0.333	28.79	**<0.001**
Tib-38	1215.48 ± 61.11	1205.23 ± 35.85	3.44 ± 3.21	0.226	12.14	**0.013**
Tib-4 Tb	247.43 ± 35.88	247.05 ± 28.27	6.03 ± 5.30	0.899	65.20	**<0.001**
Tib-4 Total	294.33 ± 39.72	294.29 ± 35.29	5.58 ± 4.93	0.990	66.75	**<0.001**
Calc Tb	226.78 ± 30.61	228.35 ± 27.22	5.60 ± 5.09	0.527	67.98	**<0.001**
Calc Total	367.75 ± 43.21	372.51 ± 44.72	5.01 ± 4.98	0.202	68.07	**<0.001**

Abbreviations: PB, phantom-based; RPL, regression-based phantomless; vBMD, volumetric bone mineral density; VOI, volumes of interest. **Bold** = Statistical significance $p<0.05$.

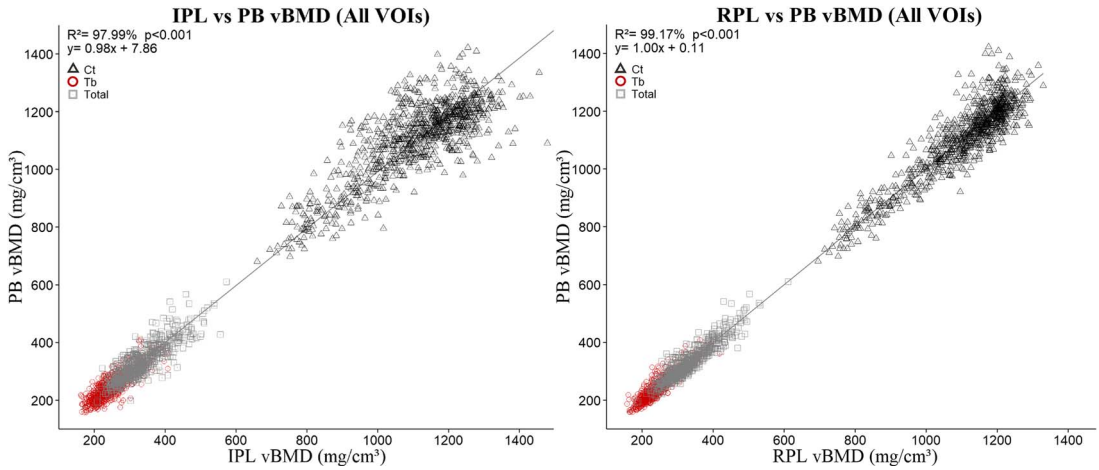

Figure 3. Univariate regressions of IPL vBMD (left) and RPL vBMD (right) compared to PB vBMD including all skeletal tissue types and sites.

between PB and IPL methods (R^2 = 87%[21] and R^2 = 99.3%,[20] respectively). However, these studies did not include a separate validation sample to determine the utility of their approach for individuals not included in the method development and lack HU thresholds to isolate bone tissue within the VOI, which may artificially lower vBMD values. Quantifying vBMD without the use of thresholds will lower measured HU and calculated density of the VOI through the inclusion of lower density marrow voxels, which may artificially strengthen the relationship between IPL and PB vBMD calibration. Furthermore, results from previous work[27] and the current study suggest that the accuracy of IPL calibration decreases when applying it to denser skeletal tissues. Direct analyses of this observation have not been performed but may provide critical insights into sources of variability that affect PL calibration methods.

When comparing both IPL and RPL calibration, results from the current study imply that both methods decrease in accuracy at skeletal VOIs of increased density (Figure 4). Larger differences in IPL compared to RPL calibration are likely associated with extrapolation from reference materials that have a lower density than all skeletal tissue types reported in this study (Table 3). Compared to previous research, the equivalent density of air from a comparable site (Table 3: Fem-50) from the Somatom Force scanner was relatively similar to reported values [Eggermont et al.: −840 (mg/cm^3) vs. Fem-50: 835.10 (mg/cm^3)], while fat and muscle EqDen varied [Eggermont et al. −80 and 30 (mg/cm^3) vs, Fem-50: −54.08 and 67.15 (mg/cm^3), respectively] (Table 3).[24] Likewise, Weaver et al. reported fat [−69 (mg/cm^3)][21] and muscle densities [77 (mg/cm^3)[21] and 85 (mg/cm^3)[23]]

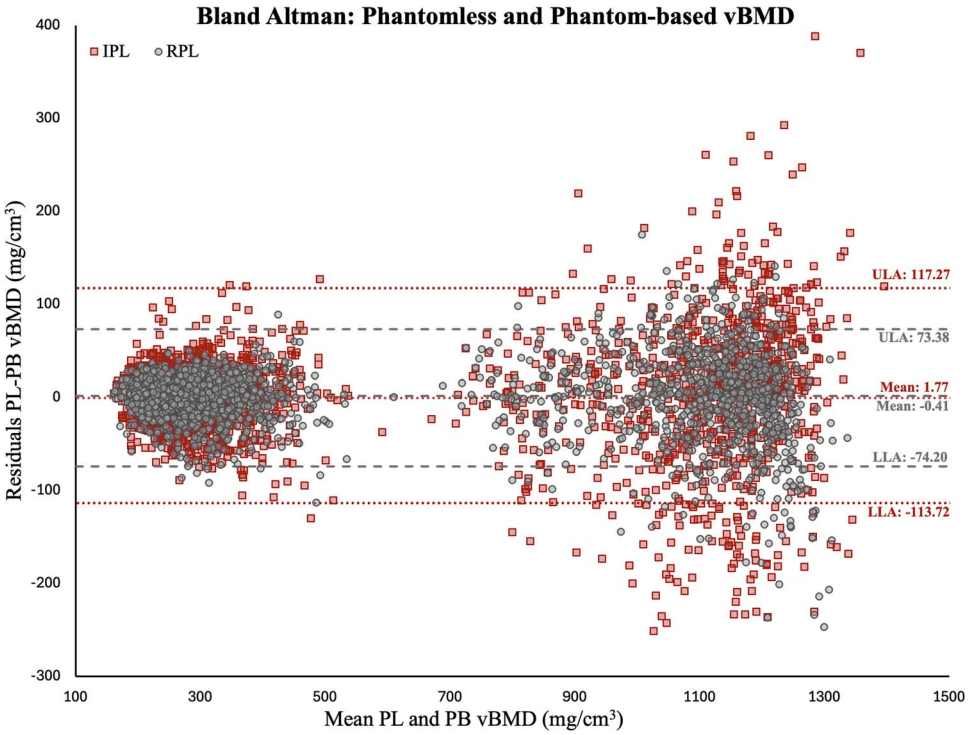

Figure 4. Bland–Altman plot of IPL (red squares, dotted lines) and RPL (gray circles, dashed lines) vBMD compared to PB vBMD. Upper and lower levels of agreement (ULA and LLA) are ±1.96 standard deviations (95% CI) from the mean PL-PB vBMD difference.

from the lumbar spine region that were outside of the range of values in the current study from L2 to L4 sites (Table 3). Error from calibration curve extrapolation may also be present in PB calibration methods if the densities of phantom rods are lower than that of the skeletal VOI. As IPL calibration techniques reported in this study and previous studies[21,23,24] utilize phantoms with known densities from 0 mg/cm^3 to 150 or 200 mg/cm^3, comparisons between vBMD derived from this alternative method may include inherent error at higher densities. As this error can potentially originate from both differential EqDen of reference materials and low-density reference phantoms, additional research is necessary to explore how changes to these parameters impact calculatedvBMD.

The exact influence of extrapolation errors from IPL and low-reference-density PB calibration was not quantified here and requires further investigation. However, as RPL calibration incorporates actual HU from the skeletal site of interest, this method may reduce extrapolation errors in calculating vBMD. As a result, it is unknown if the error between RPL and PB vBMD calibration is from the RPL method itself or from comparing RPL vBMD calibration to a PB calibration that utilizes low-reference-density phantoms, which could introduce extrapolative errors in PB calculations. Determining the source of these errors, especially for cortical bone sites, requires RPL and IPL vBMD calibration methods to be compared to PB calibration that includes low and high-density reference phantoms. For instance, the use of IPL calibration may be more severely impacted by error due to extrapolation, which can be observed in the substantially weaker relationships between IPL and PB vBMD at some of the cortical sites compared to RPL vs PB vBMD (Tables 4 and 6: Rad-30/50 and Fem-N Sup/Inf). These results suggest that vBMD at denser sites is best predicted when using methods that incorporate HU or reference densities that are similar to that of the tissue type of interest. Not only does this imply that RPL methods may be a better option for future research in PL vBMD calibration but also emphasizes the need for site specificity in development of PL methodologies.

In addition to using skeletal HU for RPL vBMD calibration, some sites included weight and height as significant predictors of PB vBMD. As relative tissue thickness influences measured density,[29] it was unsurprising to observe that weight may be a proxy measure for differential X-ray attenuation at sites of increased amounts of relative tissue thickness (ie, humerus, radius, lumbar spine, femoral neck, and femur) (Table 5). In contrast, sites with decreased relative tissue density (ie, tibia and calcaneus) only incorporated skeletal HU as a significant predictor of PB vBMD. Thus, methods for calculating vBMD in regions of increased tissue thickness/density may partially account for these variations in X-ray attenuation by including weight as a proxy measure.

The implementation of RPL and IPL vBMD calibration methods may allow for improved retrospective analyses of vBMD. Additionally, applying these methods to assess bone quality may also inform investigations of injury using finite element modeling. For example, recent research has reported similar thresholds of vertebral bone strength and fracture risk when using PB and PL vBMD calibration.[45] Likewise, finite element models of the femur constructed from both PB and PL vBMD resulted in failure loads that were not significantly different.[24] Although previous research has explored the utility of PL methods of vBMD calibration to fracture risk at specific skeletal sites, it has not been widely applied across multiple skeletal sites or tissue types despite evidence that vBMD values vary across the body[12] and should not be treated as homogenous.

In this study, both IPL and RPL methods demonstrated similar trends between PL and PB vBMD, where denser sites had weaker relationships with PB vBMD compared to less dense sites, which may be a result of extrapolative errors in calibration. However, an overall smaller magnitude and percent difference was found between RPL vBMD and PB vBMD compared to IPL vBMD. When evaluating each method overall, compared to PB vBMD, both IPL and RPL vBMD demonstrated a very strong and direct relationship with PB vBMD (R^2 = 97.99 and R^2 = 99.17%, respectively) (Figure 3), and the strength of these relationships was similar to previous studies conducting PL vBMD calibration in the lumbar spine,[21] pelvis,[20] and femur.[24] Furthermore, results from RPL calibration in this study support the use of site-specific HU regressions to calculate vBMD, which conceptually aligns with opportunistic methods of bone quality assessment that have been explored in other studies.[32,33,46,47] However, PL approaches may benefit from proxy measures for X-ray attenuation such as weight, which was used in the current study, or other variables such as tissue perimeter[20] that improve the accuracy of site-specific RPL vBMD calibration. Overall, IPL and RPL vBMD calibration both demonstrated a strong relationship to PB vBMD in males in this study, but RPL calibration had significantly smaller residual differences to PB vBMD (Figure 4). Thus, as IPL methods may have increased error from calibration extrapolation, site-specific RPL calibration may provide more accurate estimations of PB vBMD and improve the clinical and pre-clinical utility of PL methods for assessments of bone quality.

Study limitations

This study had multiple limitations that should be considered. Both the method development and validation sample only consisted of males, which may influence the results of PL reference tissue HU as tissue densities vary between sexes.[48] Furthermore, individuals in the sample were similar to the 50th percentile in height and weight; thus, the sample does not fully evaluate the effects of large differences in body size (ie, amount and distribution of tissue) even within males. Not only should future work investigate RPL calibration using height and weight with a wider range of body sizes, but the isolated relationship between demographic variables and vBMD should also be investigated with respect to each skeletal site.

This study was retrospective in nature, resulting in variability in some technical factors of CT acquisition parameters, such as reconstruction diameter and the use of multiple CT scanners. However, these fluctuations are likely more representative of discrepancies in real-world clinical data that may be accounted for within the present study. The spatial resolution of each scanner may not be sufficient to segment cortical bone in regions like the lumbar spine, calcaneus, and the distal tibia/radius due to partial volume effects. As a result, segmentation of cortical bone *within a site* was only conducted at the femoral neck due to the high contrast between the inferior/superior cortices and the trabecular compartment. For all sites, but especially cortical-only sites (midshaft humerus, radius, femur, and tibia), manual segmentation of the periosteal border was performed to avoid partial volume effects that could influence measured HU; however, this approach does not eliminate the issue entirely. As this sample is specifically intended to be more representative of CT scans within a clinical setting, the inclusion of more realistic variation may inform the utility of these methods in a real-world environment.

Both PL methods utilized within this study demonstrate a strong relationship to PB vBMD but should be further explored to confirm their potential applicability in clinical settings. In the IPL method, differences in some reference material EqDen were observed between both scanners. Although these differences were accounted for using site and scanner-specific IPL calibration, future work should explore the effects of additional manufacturers, makes, and models on EqDen values in a sample that has data collected from the same individual across multiple scanners. Both PL methods in this study demonstrated decreased accuracy at denser sites with some exceptions using RPL calibration. As these methods are compared against PB vBMD calculated using low-density phantom rods, additional studies that use phantom rods of similar density to cortical bone are recommended to isolate the effects of extrapolation to higher densities from low-reference-density phantoms.

Conclusions

PL methods to calculate vBMD provide a unique and retrospective approach to bone quality assessment. Results from this study indicate that site-specific approaches to calculating PL vBMD are necessary as the relationship between IPL/RPL vBMD and PB vBMD varied between skeletal sites and by skeletal tissue types. The differences in reference HU from which IPL and RPL calibration are developed likely affect the resulting extrapolative error within each method. Since RPL calibration is developed using HU associated with the specific skeletal site of interest and was more accurate, it may provide an advantage over IPL calibration methods. Overall, using PL methods to calculate vBMD across multiple skeletal sites increases the utility of bone quality assessments from QCT but should be conducted in a site-specific manner with respect to skeletal tissue type.

Acknowledgments

The authors thank the students, staff, and faculty of the Injury Biomechanics Research Center, especially Aditi Patel and Nicole Schipperijn. Additionally, we extend our thanks to the donors of the Ohio State University Body Donation Program for their selfless acts of research support. Finally, we also thank the United States Army Futures Command DEVCOM Analysis Center, which funded this research, as well as Michael Wassick, Kate Sandora, Aaron Alai, and David Barnes.

Author contributions

All authors were involved in the conceptualization, editing, and review of the study. Data collection, study design, analysis, and writing were performed by Z.A.H., R.L.H., A.M.A., and L.E.H.

Z.A.H. (Conceptualization, Data curation, Formal analysis, Investigation, Methodology, Resources, Supervision, Validation, Visualization, Writing—original draft, Writing—review & editing), A.M.A. (Conceptualization, Project administration, Supervision, Writing—review & editing), K.L. (Conceptualization, Funding acquisition, Project administration, Resources, Supervision, Writing—review & editing), J.Z. (Conceptualization, Methodology, Supervision, Writing—review & editing), L.E.H. (Data curation, Investigation, Writing—review & editing), and R.L.H. (Conceptualization, Project administration, Supervision, Writing—review & editing).

Supplementary material

Supplementary material is available at *JBMR Plus* online.

Funding

This study was funded by the United States Army Futures Command DEVCOM Analysis Center. All views expressed within this study are that of the authors and are not intended to reflect the views of the United States Army or the United States Army Futures Command DEVCOM Analysis Center.

Conflicts of interest

All authors agree to the contents of the submitted manuscript and declare no conflicts of interest.

Data availability

The data collected in this study were obtained at The Ohio State University. Data may be available upon reasonable request to the corresponding author.

Author statement of intent

We are providing an original research manuscript titled "Multi-site Phantomless Bone Mineral Density from Clinical Quantitative Computed Tomography in Males" for publication in the Journal of Bone and Mineral Research Plus. The research conducted in this study follows ethical guidelines and does not duplicate any other manuscripts, either published or in review.

References

1. Tarrant SM, Balogh ZJ. The global burden of surgical management of osteoporotic fractures. *World J Surg*. 2020;44(4):1009-1019. https://doi.org/10.1007/s00268-019-05237-y
2. Rashki Kemmak A, Reazpour A, Jahangiri R, Nikjoo S, Farabi H, Soleimanpour S. Economic burden of osteoporosis in the world: a systematic review. *Med J Islam Repub Iran*. 2020;2020(1):1-8. https://doi.org/10.47176/mjiri.34.154
3. Roux C, Thomas T, Paccou J, et al. Refracture and mortality following hospitalization for severe osteoporotic fractures: the Fractos study. *JBMR Plus*. 2021;5(7):e10507-e10511. https://doi.org/10.1002/jbm4.10507
4. Kanis JA, Johansson H, Odén A, et al. Characteristics of recurrent fractures. *Osteoporos Int*. 2018;29(8):1747-1757. https://doi.org/10.1007/s00198-018-4502-0
5. Lewiecki EM, Ortendahl JD, Vanderpuye-Orgle J, et al. Healthcare policy changes in osteoporosis can improve outcomes and reduce costs in the United States. *JBMR Plus*. 2019;3(9):e10192. https://doi.org/10.1002/jbm4.10192
6. Kanis JA. Diagnosis of osteoporosis and assessment of fracture risk. *Lancet*. 2004;359(9321):1929-1936. https://doi.org/10.1016/S0140-6736(02)08761-5
7. Garg M, Kharb S. Dual energy X-ray absorptiometry: pitfalls in measurement and interpretation of bone mineral density. *Indian J Endocrinol Metab*. 2013;17(2):203-210. https://doi.org/10.4103/2230-8210.109659
8. Schuit SCE, Van Der Klift M, Weel AEAM, et al. Fracture incidence and association with bone mineral density in elderly men and women: the Rotterdam study. *Bone*. 2004;34(1):195-202. https://doi.org/10.1016/j.bone.2003.10.001
9. Bolotin HH. DXA in vivo BMD methodology: an erroneous and misleading research and clinical gauge of bone mineral status, bone fragility, and bone remodelling. *Bone*. 2007;41(1):138-154. https://doi.org/10.1016/j.bone.2007.02.022
10. The American College of Radiology. *Practice Parameter For the Performance of Quantitative Computed Tomography Bone Mineral Density*. 2023:1-16. https://www.acr.org/-/media/ACR/Files/Practice-Parameters/qct.pdf.
11. Johannesdottir F, Allaire B, Bouxsein ML. Fracture prediction by computed tomography and finite element analysis: current and future perspectives. *Curr Osteoporos Rep*. 2018;16(4):411-422. https://doi.org/10.1007/s11914-018-0450-z
12. Haverfield ZA, Hunter RL, Loftis KL, Agnew AM. Skeletal site and method-dependent variability of bone mineral density in injury biomechanics research. In: *Proceedings of the IRCOBI Conference*. 2022;IRC 22(49):332-360. http://www.ircobi.org/wordpress/downloads/irc22/pdf-files/2249.pdf
13. Löffler MT, Jacob A, Valentinitsch A, et al. Improved prediction of incident vertebral fractures using opportunistic QCT compared to DXA. *Eur Radiol*. 2019;29(9):4980-4989. https://doi.org/10.1007/s00330-019-06018-w
14. Sode M, Burghardt AJ, Kazakia GJ, Link TM, Majumdar S. Regional variations of gender-specific and age-related differences in trabecular bone structure of the distal radius and tibia. *Bone*. 2010;46(6):1652-1660. https://doi.org/10.1016/j.bone.2010.02.021
15. Salzmann SN, Shirahata T, Yang J, et al. Regional bone mineral density differences measured by quantitative computed tomography: does the standard clinically used L1-L2 average correlate with the entire lumbosacral spine? *Spine J*. 2019;19(4):695-702. https://doi.org/10.1016/j.spinee.2018.10.007
16. Haverfield ZA, Agnew AM, Hunter RL. Differential cortical volumetric bone mineral density within the human rib. *J Clin Densitom*. 2023;26(2):101358. https://doi.org/10.1016/j.jocd.2023.01.002
17. Arentsen L, Hansen KE, Yagi M, et al. Use of dual-energy computed tomography to measure skeletal-wide marrow composition and cancellous bone mineral density. *J Bone Miner Metab*. 2017;35(4):428-436. https://doi.org/10.1007/s00774-016-0796-1
18. Engelke K, Lang T, Khosla S, et al. Clinical use of quantitative computed tomography-based advanced techniques in the management of osteoporosis in adults: the 2015 ISCD official positions-part III. *J Clin Densitom*. 2015;18(3):393-407. https://doi.org/10.1016/j.jocd.2015.06.010
19. Smith-Bindman R, Miglioretti DL, Johnson E, et al. Use of diagnostic imaging studies and associated radiation exposure for patients enrolled in large integrated health care systems, 1996-2010. *JAMA*. 2012;307(22):2400-2409. https://doi.org/10.1001/jama.2012.5960
20. Prado M, Khosla S, Chaput C, Giambini H. Opportunistic application of phantom-less calibration methods for fracture risk prediction using QCT/FEA. *Eur Radiol*. 2021;31(12):9428-9435. https://doi.org/10.1007/s00330-021-08071-w
21. Weaver AA, Beavers KM, Hightower RC, Lynch SK, Miller AN, Stitzel JD. Lumbar bone mineral density phantomless computed tomography measurements and correlation with age and fracture incidence. *Traffic Inj Prev*. 2015;16(sup2):S153-S160. https://doi.org/10.1080/15389588.2015.1054029
22. Michalski AS, Besler BA, Michalak GJ, Boyd SK. CT-based internal density calibration for opportunistic skeletal assessment using abdominal CT scans. *Med Eng Phys*. 2020;78(April):55-63. https://doi.org/10.1016/j.medengphy.2020.01.009
23. Weaver AA, Ronning IN, Armstrong W, et al. Computed tomography assessment of pelvic bone density: associations with age and pelvic fracture in motor vehicle crashes. *Accid Anal Prev*. 2023;193(July):107291. https://doi.org/10.1016/j.aap.2023.107291
24. Eggermont F, Verdonschot N, van der Linden Y, Tanck E. Calibration with or without phantom for fracture risk prediction in cancer patients with femoral bone metastases using CT-based finite element models. *PLoS One*. 2019;14(7):e0220564-e0220513. https://doi.org/10.1371/journal.pone.0220564
25. Hubbell JH. X-ray mass attenuation coefficients. *Int J Appl Radiat Isot*. 2004;33(11):1269-1290. Accessed April 27, 2021. https://

doi.org/10.1016/0020-708X(82)90248-4. https://www.nist.gov/pml/x-ray-mass-attenuation-coefficients
26. Hounsfield GN. Computed medical imaging. *J Comput Assist Tomogr*. 1979;4(5):665-674. https://doi.org/10.1097/00004728-198010000-00017
27. Bartenschlager S, Dankerl P, Chaudry O, Uder M, Engelke K. BMD accuracy errors specific to phantomless calibration of CT scans of the lumbar spine. *Bone*. 2021;157(December):116304. https://doi.org/10.1016/j.bone.2021.116304
28. Matheson BE, Neeteson NJ, Boyd SK. Establishing error bounds for internal calibration of quantitative computed tomography. *Med Eng Phys*. 2024;124(February):104109. https://doi.org/10.1016/j.medengphy.2024.104109
29. Yu EW, Thomas BJ, Brown JK, Finkelstein JS. Simulated increases in body fat and errors in bone mineral density measurements by DXA and QCT. *J Bone Miner Res*. 2012;27(1):119-124. https://doi.org/10.1002/jbmr.506
30. Aubrey J, Esfandiari N, Baracos VE, et al. Measurement of skeletal muscle radiation attenuation and basis of its biological variation. *Acta Physiol*. 2014;210(3):489-497. https://doi.org/10.1111/apha.12224
31. Haverfield ZA, Agnew AM, Hayden LE, Hunter RL. Region-specific equivalent densities for phantomless internal reference calibration. In: *American Society of Bone and Mineral Research Annual Conference*. 2023;38(S2):95. https://doi.org/10.1002/jbmr.4932
32. Anderson PA, Polly DW, Binkley NC, Pickhardt PJ. Clinical use of opportunistic computed tomography screening for osteoporosis. *J Bone Joint Surg*. 2018;100(23):2073-2081. https://doi.org/10.2106/JBJS.17.01376
33. Pickhardt PJ, Pooler BD, Lauder T, del Rio AM, Bruce RJ, Binkley N. Opportunistic screening for osteoporosis using abdominal computed tomography scans obtained for other indications. *Ann Intern Med*. 2013;158(8):588-595. https://doi.org/10.7326/0003-4819-158-8-201304160-00003
34. Schreiber JJ, Anderson PA, Rosas HG, Buchholz AL, Au AG. Hounsfield units for assessing bone mineral density and strength: a tool for osteoporosis management. *J Bone Joint Surg*. 2011;93(11):1057-1063. https://doi.org/10.2106/JBJS.J.00160
35. Schreiber JJ, Anderson PA, Hsu WK. Use of computed tomography for assessing bone mineral density. *Neurosurg Focus*. 2014;37(1):1-8. https://doi.org/10.3171/2014.5.FOCUS1483
36. Hunter RL, Haverfield ZA, Kang Y Seok, Agnew AM. Potential consequences of contradictions in bone mineral density assessments in injury biomechanics. In: *Proceedings of the IRCOBI Conference*. 2023;IRC 23(131):1031-1047. https://www.ircobi.org/wordpress/downloads/irc23/pdf-files/23131.pdf
37. Morsbach F, Zhang YH, Nowik P, et al. Influence of tube potential on CT body composition analysis. *Nutrition*. 2018;53(September):9-13. https://doi.org/10.1016/j.nut.2017.12.016
38. Free J, Eggermont F, Derikx L, et al. The effect of different CT scanners, scan parameters and scanning setup on Hounsfield units and calibrated bone density: a phantom study. *Biomed Phys Eng Express*. 2018;4(5). https://doi.org/10.1088/2057-1976/aad66a
39. Caksa S, Yuan A, Rudolph SE, Yu EW, Popp KL, Bouxsein ML. Influence of soft tissue on bone density and microarchitecture measurements by high-resolution peripheral quantitative computed tomography. *Bone*. 2019;124(March):47-52. https://doi.org/10.1016/j.bone.2019.04.008
40. Bartenschlager S, Cavallaro A, Pogarell T, et al. Opportunistic screening with CT: comparison of phantomless BMD calibration methods. *J Bone Miner Res*. 2023;38(11):1689-1699. https://doi.org/10.1002/jbmr.4917
41. Melton LJ, Looker AC, Shepherd JA, et al. Osteoporosis assessment by whole body region vs. site-specific DXA. *Osteoporos Int*. 2005;16(12):1558-1564. https://doi.org/10.1007/s00198-005-1871-y
42. Cataño, Jimenez S, Saldarriaga S, Chaput CD, Giambini H. Dual-energy estimates of volumetric bone mineral densities in the lumbar spine using quantitative computed tomography better correlate with fracture properties when compared to single-energy BMD outcomes. *Bone*. 2020;130(January):115100. https://doi.org/10.1016/j.bone.2019.115100
43. Boutin RD, Lenchik L. Value-added opportunistic CT: insights into osteoporosis and sarcopenia. *Am J Roentgenol*. 2020;215(3):582-594. https://doi.org/10.2214/AJR.20.22874
44. Anderson DE, D'Agostino JM, Bruno AG, Demissie S, Kiel DP, Bouxsein ML. Variations of CT-based trunk muscle attenuation by age, sex, and specific muscle. *J Gerontol*. 2013;68(3):317-323. https://doi.org/10.1093/gerona/gls168
45. Prado M, Khosla S, Giambini H. Vertebral fracture risk thresholds from phantom-less quantitative computed tomography-based finite element modeling correlate to phantom-based outcomes. *J Clin Densitom*. 2024;27(1):101465. https://doi.org/10.1016/j.jocd.2023.101465
46. Pickhardt PJ, Lee LJ, Muñoz Del Rio A, et al. Simultaneous screening for osteoporosis at CT colonography: bone mineral density assessment using MDCT attenuation techniques compared with the DXA reference standard. *J Bone Miner Res*. 2011;26(9):2194-2203. https://doi.org/10.1002/jbmr.428
47. Hendrickson NR, Pickhardt PJ, Del Rio AM, Rosas HG, Anderson PA. Bone mineral density T-scores derived from CT attenuation numbers (Hounsfield units): clinical utility and correlation with dual-energy X-ray absorptiometry. *Iowa Orthop J*. 2018;38(319):25-31
48. Grauer WO, Moss AA, Cann CE, Goldberg HI. Quantification of body fat distribution in the abdomen using computed tomography. *Am J Clin Nutr*. 1984;39(4):631-637. https://doi.org/10.1093/ajcn/39.4.631